Direct Measurement of the Area Expansion and Shear Moduli of the Human Red Blood Cell Membrane Skeleton

Guillaume Lenormand, Sylvie Hénon, Alain Richert, Jacqueline Siméon, and François Gallet
Laboratoire de Biorhéologie et d'Hydrodynamique Physico-Chimique, ESA 7057 associée au CNRS et aux Universités Paris 6 et Paris 7, Paris, France

ABSTRACT The area expansion and the shear moduli of the free spectrin skeleton, freshly extracted from the membrane of a human red blood cell (RBC), are measured by using optical tweezers micromanipulation. An RBC is trapped by three silica beads bound to its membrane. After extraction, the skeleton is deformed by applying calibrated forces to the beads. The area expansion modulus K_C and shear modulus μ_C of the two-dimensional spectrin network are inferred from the deformations measured as functions of the applied stress. In low hypotonic buffer (25 mOsm/kg), one finds $K_C = 4.8 \pm 2.7$ μN/m, $\mu_C = 2.4 \pm 0.7$ μN/m, and $K_C/\mu_C = 1.9 \pm 1.0$. In isotonic buffer, one measures higher values for K_C, μ_C, and K_C/μ_C, partly because the skeleton collapses in a high-ionic-strength environment. Some data concerning the time evolution of the mechanical properties of the skeleton after extraction and the influence of ATP are also reported. In the Discussion, it is shown that the measured values are consistent with estimates deduced from experiments carried out on the intact membrane and agree with theoretical and numerical predictions concerning two-dimensional networks of entropic springs.

INTRODUCTION

The red blood cell (RBC) is known for its ability to withstand great deformations when it passes through small capillaries. Because the inner cell is only composed of a viscous fluid (solution of hemoglobin), the resistance to stress is mainly attributed to the elastic properties of its membrane. The RBC membrane is made of a lipid bilayer reinforced on its inner face by a flexible two-dimensional protein network. This skeleton is made of spectrin dimers associated to form mainly tetramers, ~200 nm long (Bennett and Gilligan, 1993). They are linked together by complex junctions (primarily composed of actin filaments and protein 4.1) and attached to the lipid bilayer via transmembrane proteins (glycophorin C and band 3). In a simplified description, they form a triangular network in which each actin filament is connected to six spectrin tetramers. The actual spectrin network has many defects and is far from being perfectly triangular. The spectrin dimers can also self-associate into hexamers and higher-order oligomers (Liu et al., 1987; Ursitti et al., 1991). Moreover, the number of spectrin filaments per F-actin varies from three to eight (Ursitti and Wade, 1993), with an average value of six. The skeleton elasticity is determined both by the intrinsic behavior of spectrin filaments and by the topology of the network.

In the classical elastic model, the membrane response to a given stress is assumed to be linear for small deformations and is characterized by three elastic moduli: the area expansion modulus K, the shear modulus μ, and the bending stiffness B. The bending stiffness ranges from a few k_BT to a few tens of k_BT (Evans, 1983; Peterson et al., 1992), and is too small to have a noticeable influence on the membrane response to an in-plane stress. The area expansion modulus of the RBC membrane is determined by the total amount of lipids in the bilayer, and the membrane dilation under stretching is usually small. By comparison, the deformation under a shear stress is quite important and is mainly controlled by the elastic response of the spectrin network (Evans, 1973).

The elastic moduli K and μ of the membrane have been measured by various techniques, among which the micropipette is the most commonly used (Evans, 1973; Hochmuth and Waugh, 1987; Engelhardt and Sackmann, 1988; Lelièvre et al., 1995). This method leads to μ = 4-10 μN/m and K = 300-500 mN/m. More recently, by pulling on the membrane with optical tweezers, we measured $\mu = 2.5 \pm 0.4$ μN/m (Hénon et al., 1999). With this last technique, the strains are smaller than with micropipettes, which may explain the difference. However, other works based on the analysis of the local amplitude of membrane flickering can be interpreted only if μ has even a much smaller value (Peterson et al., 1992).

The present work focuses on the elastic properties of the membrane skeleton, characterized by its own area expansion modulus K_C and shear modulus μ_C. Many theoretical studies, and a few experimental ones, have been devoted to this question in the past. The goal is to separate, in the elastic behavior of the entire RBC membrane, the respective roles of the lipid bilayer and of the spectrin network. Depending on whether the skeleton is free or bound to the lipid bilayer, theoretical approaches are slightly different. For a triangular network constrained to in-plane deformations, analytical and numerical works have predicted that the ratio K_C/μ_C should be equal to 2 in the small stress regime (Kantor and Nelson, 1987; Boal et al., 1993; Hansen et al., 1996). This result holds whether the spectrin strands are

Received for publication 16 October 2000 and in final form 28 March 2001.

Address reprint requests to Dr. Sylvie Hénon, LBHP Case 7056, 2 Place Jussieu, F-75251 Paris Cedex 5, France. Tel.: 33-1-4427-7782; Fax: 33-1-4427-4335; E-mail: henon@ccr.jussieu.fr.

0006-3495/01/07/43/14 $2.00

modeled as Hookean springs or are submitted to square-well interactions. Moreover, simulations have shown that the elastic moduli decrease when adding topological defects, either by increasing the number of high-order oligomers or by decreasing the coordinance number per complex junction (Hansen et al., 1997). However, an unbound network fluctuates out of its average plane, which reduces the average distance between vertices and modifies the elastic coefficients as compared to a plane network. By performing Monte Carlo simulations on a network freely fluctuating in a half-space, Boal (1994) has shown that the ratio of the in-plane elastic moduli may drop to 1.7. Furthermore, it has been shown that the Poisson ratio of a two-dimensional network may become negative at large stress (Aronovitz and Lubensky, 1988; Boal et al., 1993), but this regime falls out of most of the usual experimental conditions (including the ones reported in this paper).

In earlier experiments, the RBC membrane was deformed by aspiration into a micropipette. Although the skeleton remains bound to the membrane in this case, it can freely slide along the lipid bilayer and therefore sustains both shear and expansion strains. Mohandas and Evans (1994) have proposed that the overall shear modulus μ of the membrane is related through a serial coupling to the area expansion K_C and shear modulus μ_C of the skeleton, as $\mu \sim (\mu_C K_C)/(\mu_C + K_C)$. According to this formula, one expects μ and μ_C to have the same order of magnitude. Independently, Stokke et al. (1986) predicted that the projection length aspirated inside the pipette strongly depends on the ratio μ/K_C. Moreover, by analyzing fluorescence images of the spectrin distribution inside the pipette, Discher et al. (1994) inferred a first measurement of the ratio K_C/μ_C, close to 2.

Qualitative behavior of a free, freshly extracted RBC membrane skeleton has also been reported in the literature (Svoboda et al., 1992). In that study, a membrane skeleton trapped with optical tweezers was extracted under a microscope and deformed in a flow field. From the extent of thermal undulations and from the skeleton deformability, the skeleton bending rigidity appeared to be markedly lower than that of the intact RBC membrane. Moreover, a great dependence of the skeleton size on the ionic strength was highlighted.

In this work we present new experiments and data concerning the elastic behavior of the isolated membrane skeleton. We measure both K_C and μ_C by means of optical tweezers. Our experimental setup does not allow us to measure the skeleton bending stiffness B_C. Small silica beads bound to the skeleton are used as handles to seize and manipulate it after dissolving the lipid bilayer with a detergent (Yu et al., 1973). By applying calibrated stresses to the skeleton through the beads and simultaneously measuring its deformation, we can determine K_C and μ_C. In a low osmolarity buffer, we find $\langle K_C \rangle = 4.8 \pm 2.7$ μN/m, $\langle \mu_C \rangle = 2.4 \pm 0.7$ μN/m, and $\langle K_C/\mu_C \rangle = 1.9 \pm 1.0$. These values are in good agreement with the expected ones. The skeleton shear modulus μ_C has the same order of magnitude as the membrane shear modulus μ measured by optical tweezers (Hénon et al., 1999). The ratio $\langle K_C/\mu_C \rangle$ is close to values obtained by theoretical and numerical studies (Boal, 1994; Hansen et al., 1996). We also measure K_C and μ_C in an isotonic buffer to evaluate the influence of the ionic strength. Finally, we characterize the time evolution of the skeleton stiffness in either low osmolarity or isotonic buffers.

MATERIALS AND METHODS

Optical tweezers

Our optical tweezers setup has been described elsewhere (Hénon et al., 1999). Schematically, tweezers are made by focusing a high-power infrared laser beam (Nd:YAG, $\lambda = 1.064$ μm, $P_{max} = 600$ mW) through the immersion objective ($\times$100, NA = 1.25) of a standard optical microscope. At the converging point, the electric field is large enough to trap small dielectric objects, in the present work spherical silica beads, 2.1 μm in diameter. The trap is located in the same plane as the observation plane of the microscope. Two galvanometric mirrors having perpendicular axes are used to control the trap position or to create multiple traps by rapidly commuting the focusing point between different positions at frequency f_c ($f_c \sim 200$ Hz). They are monitored by a numerical program coupled to the NIH Image analysis software. This program can handle the positions of multiple traps (up to four).

The restoring force F exerted on a trapped bead depends on the departure $\Delta x = x - x_0$ of the bead position x from the trap center x_0. Following Simmons et al. (1996), $F(\Delta x)$ is calibrated by applying a known viscous drag force to the bead. Practically, the calibration chamber is made of a microscope slide and coverslip separated by a plastic film spacer and is mounted on a piezoelectric stage (model P-780; PolytecPI, Waldbronn, Germany). The chamber is filled with a suspension of beads in pure water and moved back and forth at constant velocity v in the horizontal plane, while one bead is trapped by the laser beam held at a fixed position x_0. Because the steady-state regime is reached in a few microseconds and the bead inertia is negligible, the trapping force $F(\Delta x)$ exactly equilibrates the viscous drag force $F' = 6\pi\eta R v$, where $R = 1.05$ μm is the bead radius and $\eta = 0.9\ 10^{-3}$ Pa·s is the water viscosity at the experimental temperature $T \sim 25$°C. A correction is made to the viscous drag force to take into account the finite distance from the bead to the top or bottom of the chamber (Svoboda and Block, 1994). The bead displacement in the flow field Δx is measured from the microscope image. We find that $F(\Delta x)$ is proportional to Δx at least for $\Delta x < 1$ μm, meaning that the trap is harmonic in this range. In a good approximation, F is found proportional to the incident laser power P, so that one can write:

$$F = \alpha_n A P \Delta x \qquad (1)$$

We measured the coefficient A for a single trap: $A = 0.26$ pN mW^{-1} μm^{-1}. The numerical constant α_n depends on the number n of traps. By definition, α_1 is equal to 1, and we found $\alpha_2 = 0.40$, $\alpha_3 = 0.25$, $\alpha_4 = 0.18$. We noticed no dependence of A and α_n on the commuting frequency f_c in the range 150 Hz $< f_c <$ 300 Hz. Their dependence with the distance h between the trap and the top coverslip is weak in our experimental situation (10 μm $< h <$ 60 μm).

Flow chamber

A schematic drawing of the stainless steel flow chamber is shown in Fig. 1. The flow is limited by a coverslip and a cylindrical lens. The chamber

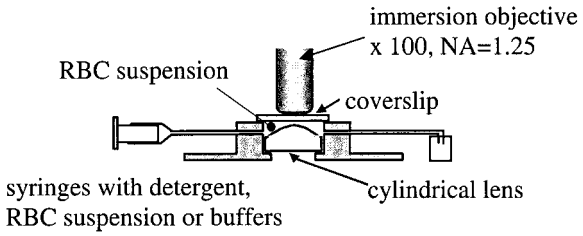

FIGURE 1 Scheme of the stainless steel flow chamber, placed on the stage of the microscope. The RBCs are trapped in the narrow channel ($e \sim 60\ \mu m$) limited by the cylindrical lens and the coverslip. The immersion objective is used both for the observation and the optical tweezers focusing. Several holes allow local injection of buffers, detergent solution, and RBC suspension through small polyethylene catheters (not shown).

inner volume is ~ 0.7 ml. The lens has negligible effect on the path of optical rays, its role is to make a narrow channel ($50\ \mu m < e < 80\ \mu m$) to trap the RBCs as close as possible to the top coverslip. The chamber is placed on the microscope stage and is illuminated from below for bright-field observation. The laser beam is focused into the flow field through the top objective and coverslip. Several holes are drilled in the chamber walls to inject the RBCs' suspension, the buffers, and the detergent solution through small polyethylene catheters (300 μm in diameter).

Solutions are injected at controlled rates using syringe pumps. A thermocouple probe measures the temperature in the chamber. The cylindrical lens is coated with octadecyltrichlorosilan (Sigma, Paris, France) after a meticulous cleaning (Decon 90 at 60°C for 20 min, H_2O_2 with H_2SO_4 for 10 min, and O_3 for 1 h). Moreover, 2 ml of a solution of 50 mg/ml bovine serum albumin (BSA; Sigma A 4503) diluted in phosphate buffered saline (PBS; Sigma P 4417), are injected at the beginning of the manipulation. This treatment prevents beads, erythrocytes, and (partially) freshly extracted skeletons from sticking to the lens.

Extraction of the skeleton

Fresh blood is obtained by fingertip needle prick. Red blood cells are suspended in PBS, then washed three times by centrifugation. Silica microbeads ($\sim$1 bead per RBC) are added to the suspension. After incubating for 1 h at 4°C, the beads stick spontaneously and irreversibly to the RBC membrane (from zero to five beads bind to each RBC). After adding a small amount of BSA (1 mg/ml), the suspension is slowly injected into the flow chamber. We select an RBC with three beads attached to its periphery and trap the beads with three optical tweezers (see Fig. 2). Although no special treatment is made to obtain ghosts, most of the cells carrying several beads appear partially lysed when entering into the flow chamber: the shear stresses applied to the membrane by the beads during the injection are probably large enough to tear it. Consequently, the skeletons are extracted from ghosts most of the time.

Two different kinds of manipulation are held: the first one in a hypotonic buffer (5 mM NaCl, 5 mM K_2HPO_4, pH 7.4, 25 mOsm/kg) and the second one in an isotonic buffer (PBS: 8.1 mM Na_2HPO_4, 1.5 mM $KHPO_4$, 2.7 mM KCl, and 137 mM NaCl, pH 7.4, 300 mOsm/kg). For the low osmolarity experiments, once the RBC is seized by the three beads, the hypotonic buffer is slowly injected for 5 min to lower the osmolarity of the medium. Then the detergent solution (Triton X-100 in hypotonic buffer $\sim$ 1–3‰ in volume) is injected until bilayer dissolution. Afterward, the detergent is rinsed out with a second injection of hypotonic buffer for 10 min. The injected volume roughly equals the chamber volume, so that the osmolarity is stabilized at 25 mOsm/kg. Isotonic buffer experiments begin by the injection of the detergent (Triton X-100 in PBS $\sim$ 1–3‰ in volume). After the membrane dissolution, PBS is injected for 5 min to rinse out the detergent.

We have performed independent tests to check that the membrane dissolution is totally achieved. Following the method described by Discher et al. (1994), we have labeled the membrane bilayer with a fluorescent lipophilic probe (DIOC18, from Molecular Probes, Eugene, OR), and we have checked that the fluorescence signal vanishes completely in a few seconds after the beginning of the detergent injection.

We start to manipulate the membrane skeleton 5 or 10 min after its extraction. All the manipulations take place at 25°C, measured in the flow chamber. We cannot measure the actual temperature of the skeleton, but we assume that the local heating due to the tweezers is negligible (Liu et al., 1995; Hénon et al., 1999) because the absorption of the skeleton proteins at $\lambda = 1.064\ \mu m$ is very low.

Once the bilayer is dissolved, the RBC is no longer visible in bright field, but we observe in most cases that the beads cannot be moved independently; this indicates that the beads remain linked together through the skeleton and that their adherence sites on the RBC are most of the time transmembrane proteins linked to the skeleton, i.e., glycophorin or band 3. Several experiments are performed after labeling the F-actin with a fluorescent probe (phalloidin-TRITC) to check that the skeleton remains intact after extraction and to visualize it during its deformation (see corresponding section and Fig. 5). Although it is reported that the labeling procedure does not change the elastic properties of the skeleton (Discher et al., 1994), all the measurements are realized without the fluorescent labeling.

Deformations of the skeleton

The skeleton is deformed by varying the distances between the traps. Three different kinds of deformation are carried out. By increasing the distances between the traps simultaneously in two orthogonal directions, we generate a deformation close to pure area expansion. By increasing the distance in only one direction, we exert both area expansion and shear. The third kind of deformation is obtained by increasing the distance in one direction and decreasing it in the other direction. Generally, this leads to a deformation close to pure shear. We increase the distance between the traps by steps of $\sim 0.1\ \mu m$. Within a few minutes, we submit the skeleton to several cycles corresponding to the three different kinds of deformation, each cycle being made of five to eight successive steps of increasing stress, followed by a symmetric decrease. Because the skeleton is invisible, its deformation is interpolated from the bead positions (see the following section and Theory). To study a possible time evolution (up to 45 min after extraction), several sets of measurements alternate with 10–15-min waiting periods.

Visualization, force measurements, and data analysis

Visualization and image recording are made with a video camera (model SIT 68, Dage-MTI Inc., Michigan City, IN) connected to a Macintosh computer. For each configuration of the traps, an image is recorded. The position of the center of each bead is located with the NIH Image analysis software, with an accuracy of 50 nm. To determine the traps' positions, free isolated beads are trapped afterward at equilibrium in each of the three tweezers for several trap configurations corresponding to the actual cycles of the skeleton deformation; in these conditions, the positions of the bead centers and of the traps are identical. The calibration formula 1 gives the force exerted on each bead during the skeleton manipulation. For all measurements, the laser power is set to 150 mW; the force applied to each bead varies from 1 to 8 pN. The uncertainty comes both from the determination of the bead and trap relative positions and from the accuracy on force calibration. We evaluate the final uncertainty on the force measurements to $\sim$15%. Similarly, the uncertainty on the beads positions determines the error bars on the skeleton deformation (10% on average). To calculate the

strain, the shear and area expansion stress, and finally to get the moduli μ_C and K_C, the data analysis and graphic Kaleidagraph software (Synergy Software, Reading, PA) is used. The corresponding algebra is developed in the Theory section.

Membrane skeleton labeled with phalloidin-TRITC

Control images of the actual deformation of the skeleton are done by labeling F-actin with phalloidin-TRITC (Sigma, P1951). The method used is described in Discher et al. (1994). It uses a cold, hypotonic lysis, so that fluorescent probes can enter the cell and bind internally. Briefly, 2.5 μl phalloidin-TRITC are dissolved in 20 μl cold lysis buffer (10 mM sodium phosphate, pH 7.4). Cold, packed red cells (5 μl) are added and after 10 min, the suspension is adjusted to 100 mM KCl, 1 mM $MgCl_2$, and incubated at 37°C for 30 min. Then, the RBCs are washed by centrifugation and the silica beads are added.

THEORY

In this section we determine quantitative relations, involving the elastic moduli K_C and μ_C, between the forces exerted by each of the three trapped beads and the stresses and strains applied to the membrane skeleton.

We consider the membrane skeleton as a continuous, homogeneous, and isotropic elastic medium. Although out-of-plane fluctuations may be allowed, the skeleton is assumed to be flat, on average, as soon as it is put under a slight tension. Then its in-plane elastic properties are characterized by a two-dimensional area expansion modulus K_C and shear modulus μ_C. These approximations are reasonable because both the membrane thickness (a few nanometers) and the mesh size (~200 nm) are small compared to the scale of experimental deformations (a few micrometers). We also neglect the bending elasticity. Finally, we only consider small deformations, so that linear elastic theory applies.

A scheme of the deformed and undeformed skeleton is represented in Fig. 2. It is assumed that the three trapping forces $\mathbf{F}_A$, $\mathbf{F}_B$, and $\mathbf{F}_C$ are exerted at the centers A, B, and C of the beads. We restrict the study of the skeleton deformation in the region limited by the triangle ABC. Calculating the exact strain and stress everywhere would require extra numerical analysis. In a simplified analytical approach, we assume that the stress (and the strain) is homogeneous over the region ABC, so that it keeps its triangular shape, becoming A′B′C′ under tension. We are aware of the fact that the actual stress may not be homogeneous everywhere, especially in the regions where the skeleton sticks to the beads. This is a source of uncertainty in the determination of the elastic moduli. Images of deformed fluorescent RBCs were precisely taken to evaluate this effect, from which we conclude that the assumption of a homogeneous stress is reasonable.

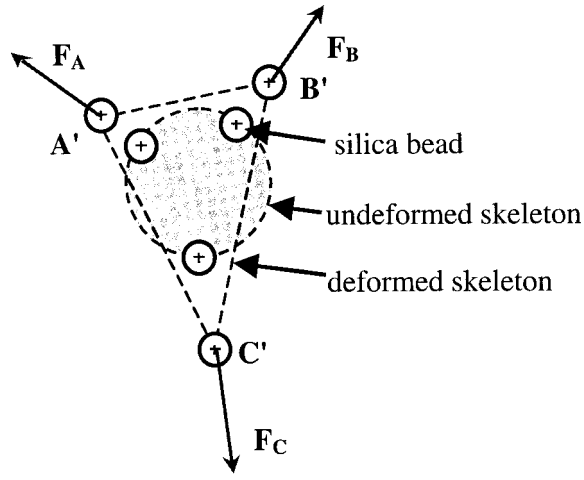

FIGURE 2 Principle of the experimental procedure (not to scale). An RBC is seized by trapping each of the three silica beads bound to its periphery in optical tweezers. A detergent solution is injected to dissolve the lipid bilayer. The beads remain stuck to the skeleton. The skeleton is deformed by varying the distances between the traps. Its deformation, interpolated from the beads positions, is a superposition of shear and area expansion. The forces exerted on the beads are calculated with calibration formula 1.

In the linear theory of elasticity, Hooke's law describes the relation between the two-dimensional 2×2 stress tensor [$\boldsymbol{\sigma}$] and strain tensor [$\mathbf{u}$]. In the principal system of coordinates, in which these tensors are diagonal, this relation is written as:

$$\sigma_{XX} = K_C(u_{XX} + u_{YY}) + \mu_C(u_{XX} - u_{YY}) = \sigma_e + \sigma_s \quad (2a)$$

$$\sigma_{YY} = K_C(u_{XX} + u_{YY}) - \mu_C(u_{XX} - u_{YY}) = \sigma_e - \sigma_s \quad (2b)$$

$$\sigma_{XY} = 2\mu_C u_{XY} = 0$$

Here σ_e and σ_s are, respectively, defined as the pure area expansion stress and the pure shear stress components. To analyze the experiments, the procedure is the following: one has to relate on the one hand the forces $\mathbf{F}_A$, $\mathbf{F}_B$, and $\mathbf{F}_C$ to the stress components σ_e and σ_s, and on the other hand the deformation of the triangle ABC into A′B′C′ to the strain components u_{XX} and u_{YY}. Then K_C and μ_C are determined by Eqs. 2a and 2b.

The first step consists of splitting the triplet ($\mathbf{F}_A$, $\mathbf{F}_B$, $\mathbf{F}_C$) into two triplets of forces ($\mathbf{F}_e$) = ($\mathbf{F}_{eA}$, $\mathbf{F}_{eB}$, $\mathbf{F}_{eC}$) and ($\mathbf{F}_s$) = ($\mathbf{F}_{sA}$, $\mathbf{F}_{sB}$, $\mathbf{F}_{sC}$), applied to the vertices A, B, and C, and respectively generating a pure area expansion stress and a pure shear stress. This splitting can be made through a geometrical construction detailed in the Appendix. To summarize it, one projects $\mathbf{F}_A = \mathbf{F}_{AB} + \mathbf{F}_{AC}$ along the two directions normal to AB and AC (see Fig. 3) and makes equivalent projections in B and C. The triplets ($\mathbf{F}_e$) and ($\mathbf{F}_s$)

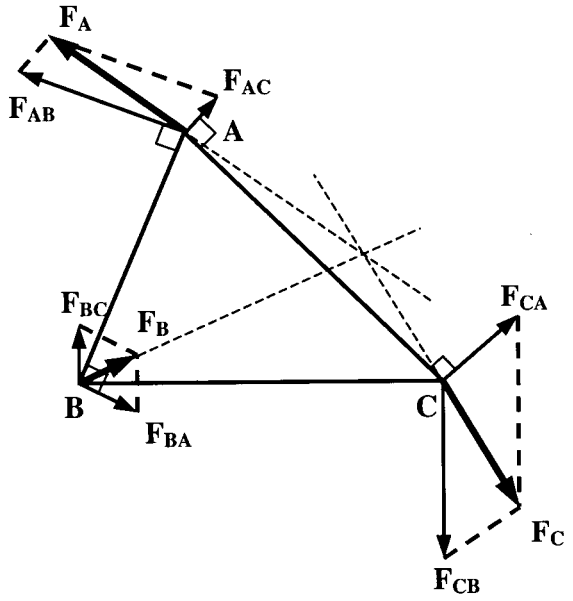

FIGURE 3 Construction used to separate the triplet of forces $(\mathbf{F}) = (\mathbf{F}_A, \mathbf{F}_B, \mathbf{F}_C)$ into two triplets of forces $(\mathbf{F}_e) = (\mathbf{F}_{eA}, \mathbf{F}_{eB}, \mathbf{F}_{eC})$ and $(\mathbf{F}_s) = (\mathbf{F}_{sA}, \mathbf{F}_{sB}, \mathbf{F}_{sC})$, respectively, generating a pure area expansion and a pure shear stress. $\mathbf{F}_A = \mathbf{F}_{AB} + \mathbf{F}_{AC}$ is projected along the two directions normal to AB and AC. Equivalent projections are drawn in B and C. The triplets $(\mathbf{F}_e)$ and $(\mathbf{F}_s)$ are explained in the text.

are then given by:

$$\mathbf{F}_{eA} = -\frac{\mathbf{F}_{BC} + \mathbf{F}_{CB}}{2}$$

$$\mathbf{F}_{sA} = \frac{\mathbf{F}_A - \mathbf{F}_{BA} - \mathbf{F}_{CA}}{2} = \mathbf{F}_A - \mathbf{F}_{eA} \qquad (3a)$$

$$\mathbf{F}_{eB} = -\frac{\mathbf{F}_{AC} + \mathbf{F}_{CA}}{2}$$

$$\mathbf{F}_{sB} = \frac{\mathbf{F}_B - \mathbf{F}_{CB} - \mathbf{F}_{AB}}{2} = \mathbf{F}_B - \mathbf{F}_{eB} \qquad (3b)$$

$$\mathbf{F}_{eC} = -\frac{\mathbf{F}_{AB} + \mathbf{F}_{BA}}{2}$$

$$\mathbf{F}_{sC} = \frac{\mathbf{F}_C - \mathbf{F}_{AC} - \mathbf{F}_{BC}}{2} = \mathbf{F}_C - \mathbf{F}_{eC} \qquad (3c)$$

The relations among σ_e, σ_s, $(\mathbf{F}_e)$, and $(\mathbf{F}_s)$ are:

$$\sigma_e = 2\frac{F_{eA}}{BC} = 2\frac{F_{eB}}{AC} = 2\frac{F_{eC}}{AB}$$

(see Eq. A8)

$$\sigma_s = 2\frac{F_{sA}}{BC} = 2\frac{F_{sB}}{AC} = 2\frac{F_{sC}}{AB}$$

(see Eqs. A10–A12)

The strain may be calculated from the measured deformation of the triangle ABC into A′B′C′. The pure area expansion contribution $u_{XX} + u_{YY}$ is equal to the relative surface increase $\Delta S/S$ of the triangle. The area expansion modulus is given by $\sigma_e = K_C \Delta S/S$.

The shear deformation is defined as $u_{xx} - u_{yy} = \partial u_x/\partial x - \partial u_y/\partial y$, where $\mathbf{u}$ represents the local displacement. It can easily be calculated in the principal system of coordinates $(\mathbf{e}_X, \mathbf{e}_Y)$ defined in the Appendix, in which $\partial u_X/\partial Y = \partial u_Y/\partial X = 0$. For instance, in this system of coordinates, the side $\mathbf{AB} = X\mathbf{e}_x + Y\mathbf{e}_x$ becomes $\mathbf{A'B'} = X'\mathbf{e}_x + Y'\mathbf{e}_x$ and the shear deformation is given by:

$$u_{XX} - u_{YY} = \frac{X' - X}{X} - \frac{Y' - Y}{Y} \qquad (4)$$

The shear modulus is obtained by $\sigma_s = \mu_C(u_{XX} - u_{YY})$.

To conclude this section, it is important to point out that the membrane skeleton is a closed surface and that its deformation depends on the relative positions of the beads at its periphery. If the plane defined by the three beads is a plane of symmetry for the RBC, the forces are symmetrically exerted on both sheets of the skeleton (Fig. 4 *A*). On the contrary, if it is not a plane of symmetry, only one sheet (the top or the bottom one) is deformed (Fig. 4 *B*). The

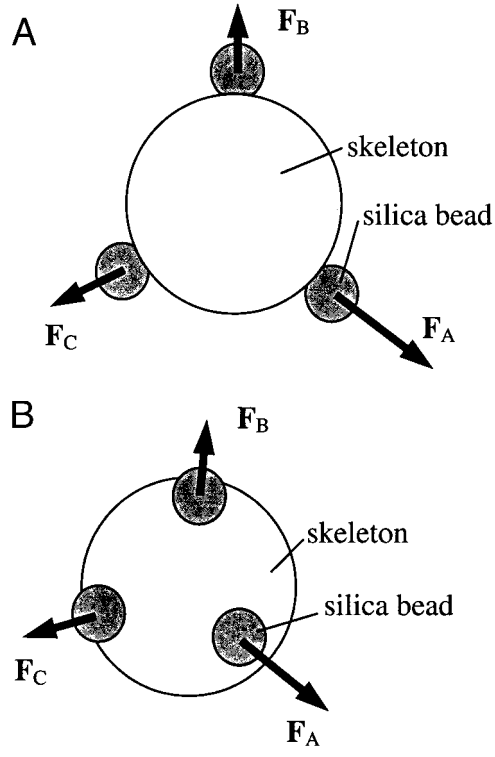

FIGURE 4 The number of sheets of the skeleton that are deformed depends on the position of the beads. (*A*) If the beads are in a plane of symmetry for the skeleton, the upper and lower sheets of the skeleton are deformed. (*B*) If the beads are not in a plane of symmetry, only one sheet is deformed.

above theoretical presentation is restricted to a single sheet, but the possibility of pulling simultaneously on both sheets will be taken into account in the Results section.

RESULTS

Visualization of the skeleton

Control images of the skeleton after its extraction are done by labeling F-actin with phalloidin-TRITC, allowing visualization of the skeleton during its deformation. Experiments are carried out in hypotonic and isotonic buffer. Fig. 5 shows two images taken during the first set of deformations in isotonic buffer. Fig. 5 *A* is taken with low stress applied to the skeleton, Fig. 5 *B* shows the same skeleton at higher stress. They confirm that the skeleton remains stuck to the beads after the dissolution of the lipid bilayer. Moreover, the deformed skeleton globally keeps a triangular shape on both images: no local excessive stretching is visible in Fig. 5 *B*, especially in the regions where the beads are attached. This indicates that, in a first approximation, the stress is homogeneous over the deformed area and validates the model proposed in the Theory section. Images of deformed skeletons in hypotonic buffer lead to the same conclusion.

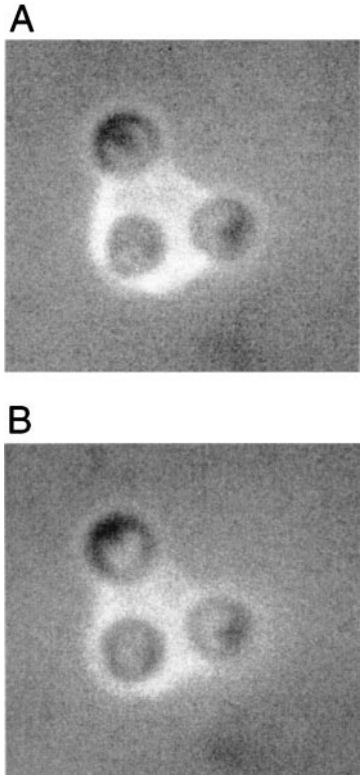

FIGURE 5 Two images of a skeleton visualized by labeling F-actin with phalloidin-TRITC, taken during the first set of deformations in an isotonic buffer. In (*A*) a low stress is applied to the skeleton, and (*B*) shows the same skeleton at higher stress. The skeleton roughly keeps a triangular shape, meaning that the approximation of homogeneous strain is reasonable.

Measurements in low osmolarity buffer

We present here measurements held in a low osmolarity buffer (25 mOsm/kg) without adenosine triphosphate (ATP) and at room temperature, i.e., ~25°C. In this section we report the results of the first set of skeleton manipulations, which starts 10 min after its extraction and takes place within a couple of minutes. A low osmolarity buffer is used to prevent the shrinkage of the skeleton in the presence of screening charges, as reported by Svoboda et al. (1992).

Before extraction, the RBC membrane is maintained under a slight tension by pulling on the beads with the optical

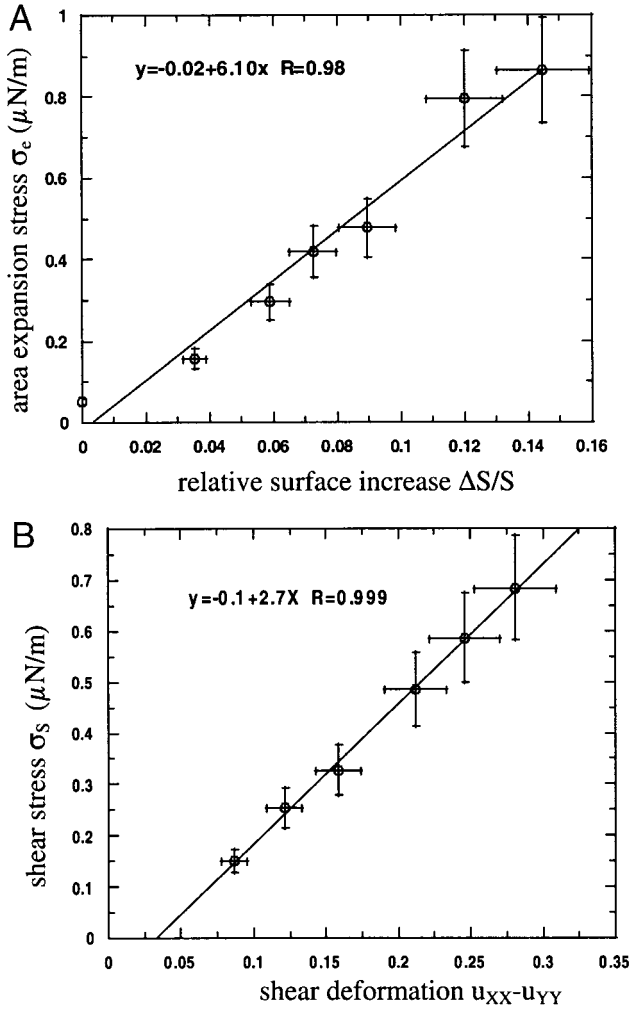

FIGURE 6 Stress versus strain plotted for a typical deformation of a freshly extracted skeleton in low osmolarity buffer (25 mOsm/kg). (*A*) Pure area expansion component σ_e versus area dilation $\Delta S/S$; (*B*) pure shear component σ_s versus shear strain $u_{XX} - u_{YY}$. Notice the linear behavior in both cases, in agreement with linear elasticity model. The respective slopes give the area expansion modulus K_C and the shear modulus μ_C.

tweezers. When the front of the detergent solution arrives on the trapped RBC, the membrane begins to deform. Then, within a second, the beads move back to the center of the traps while the contour of the RBC disappears. This means that, in hypotonic buffer, the skeleton slightly expands as the lipid bilayer is dissolved (see Discussion). Fig. 6 *A* and *B* show typical results obtained for a deformation consisting of increasing the distance between the traps along one direction while the distance along the perpendicular one remains constant. This deformation generates both area expansion and shear strains. Graph 6 *A* is a plot of the area expansion stress σ_e versus the relative surface increase $\Delta S/S$. Graph 6 *B* shows the shear stress σ_s versus the shear strain $u_{XX} - u_{YY}$. We observe a linear relation in both cases, which means that the skeleton elastic behavior is correctly described by Hooke's law. On graph 6 *A*, the area increases by up to 15%. The slope gives the area expansion modulus, here $K_C = 6.1$ μN/m. On graph 6 *B*, the maximum deformation is 30%, and the slope gives the shear modulus $\mu_C = 2.7$ μN/m.

Table 1 reports the values of the shear and area expansion moduli, obtained for 19 different skeletons in the 25 mOsm/kg buffer. Each value is an average over several measurements corresponding to different deformations (usually six) of the same skeleton. The values of the elastic coefficients, averaged over the 19 skeletons, are $\langle K_C \rangle = 9.0 \pm 3.6$ μN/m, $\langle \mu_C \rangle = 5.2 \pm 2.1$ μN/m, and $\langle K_C/\mu_C \rangle = 2.3 \pm 1.1$. Notice the important dispersion: 3.5 μN/m $< K_C <$ 14.6 μN/m, 1.8 μN/m $< \mu_C <$ 9.6 μN/m, and $1.0 < K_C/\mu_C < 4.8$. It can be explained by the fact that we do not control the number of sheets of the skeleton that are actually deformed. In a simple description, the forces are exerted either on a single sheet of the skeleton or on both sheets, depending on the bead positions (see Fig. 4). The actual situations may be more complex and, for instance, the deformation of the same skeleton may concern either the two sheets or only a single one, depending on the direction of the exerted forces. Of course, when two sheets are deformed, one expects to measure apparent elastic moduli twice as much as for a single sheet. To take this into account, we have plotted in Fig. 7, *A* and *B*, the values obtained for each single deformation (77 measurements for K_C and 76 for μ_C). As expected, the stack histograms $N(K_C)$ and $N(\mu_C)$ present two maxima. For instance, in Fig. 7 *A*, the first maximum is at $K_C \sim 4-6$ μN/m and the second one at $K_C \sim 9-11$ μN/m. The ratio between these values is close to 2, which supports our assumption about the deformation of either one or two sheets. To be more quantitative, we fit the histogram by a sum of two Gaussian curves:

$$N(K_C) = A_1 \exp\left(-\frac{(K_C - \langle K_C \rangle)^2}{2\Delta K_{C1}^2}\right) + A_2 \exp\left(-\frac{(K_C - 2\langle K_C \rangle)^2}{2\Delta K_{C2}^2}\right) \quad (5)$$

where A_1 and A_2 are two constants, ΔK_{C1} and ΔK_{C2} the standard deviations. The maximum of the second Gaussian function is set to twice the first one. The same analysis is performed for the shear modulus μ_C, for which the stack

TABLE 1 Area expansion modulus and shear elastic modulus measured for 19 skeletons in low osmolarity buffer (25 mOsm/kg) without ATP

Skeleton No.	Area Expansion Modulus K_C (μN/m)	Shear Modulus μ_C (μN/m)	K_C/μ_C
1	7.1 ± 3.6(6)	3.7 ± 2.4(6)	2.0 ± 0.6(6)
2	4.4 (1)	6.3 ± 1.3(2)	—
3	12.3 ± 5.4(3)	—	—
4	10.2 ± 3.8(5)	8.8 ± 3.9(4)	1.5 ± 0.8(4)
5	8.4 ± 2.7(6)	4.5 ± 0.8(4)	1.9 ± 1.1(4)
6	4.1 ± 1.3(6)	—	—
7	9.3 ± 2.6(6)	4.8 ± 1.5(6)	2.0 ± 0.2(6)
8	11.9 ± 6.1(4)	8.1 ± 3.3(4)	—
9	6.8 ± 1.5(8)	4.5 ± 2.7(8)	2.0 ± 1.3(8)
10	3.5 ± 1.1(7)	3.9 ± 1.4(7)	1.1 ± 0.8(7)
11	9.7 ± 3.7(3)	4.0 ± 1.5(2)	2.0 ± 0.1(2)
12	14.6 ± 4.8(4)	7.3 ± 4.6(6)	3.4 ± 2.0(3)
13	14.0 ± 2.2(3)	4.5 ± 1.4(5)	3.0 ± 1.2(3)
14	6.5 ± 0.5(4)	3.5 ± 1.8(4)	2.3 ± 1.1(4)
15	13.9 ± 1.4(7)	9.6 ± 3.2(3)	1.5 ± 0.6(3)
16	—	5.5 ± 3.7(3)	—
17	12.2 ± 1.7(5)	3.6 ± 1.2(4)	3.7 ± 0.8(4)
18	4.3 ± 3.3(4)	4.1 ± 0.9(4)	1.0 ± 0.7(4)
19	8.7 ± 3.6(6)	1.8 ± 0.6(4)	4.8 ± 0.7(4)
Average	9.0 ± 3.6	5.2 ± 2.1	2.3 ± 1.1

The values are averaged over several deformations exerted on the same skeleton (number indicated in parentheses).

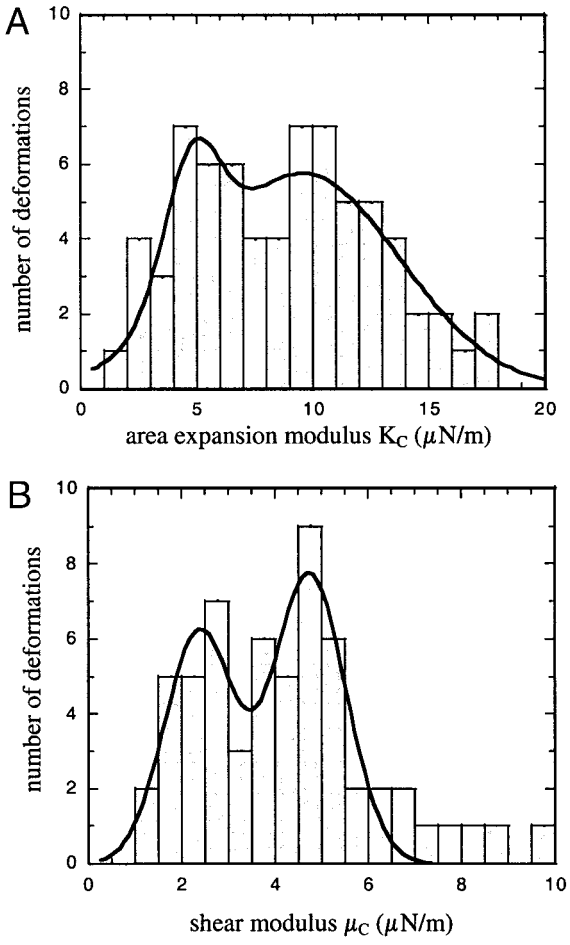

FIGURE 7 Stack histograms of the elastic moduli K_C (*A*) and μ_C (*B*) obtained for each deformation (77 measurements for K_C and 76 for μ_C on 19 different skeletons) right after extraction in low osmolarity buffer. The histograms present two maxima: the first one corresponds to the deformation of a single sheet of the skeleton and the second one of both sheets. The values of the two maxima are in a 2:1 ratio. The best fit with a double Gaussian is also represented.

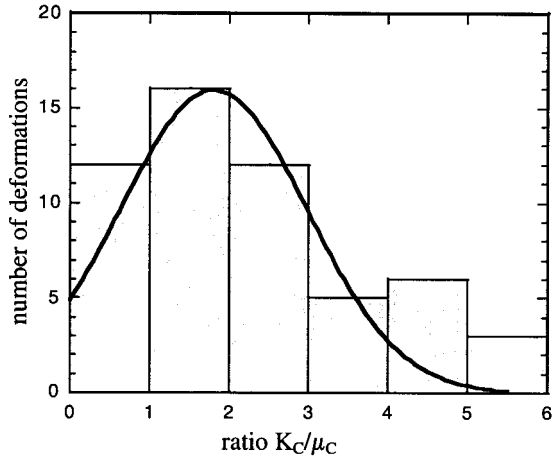

FIGURE 8 Stack histogram of the ratio K_C/μ_C, K_C, and μ_C being measured from the same deformation of a skeleton, right after extraction in low osmolarity buffer. The best Gaussian fit is shown. The center value is $\langle K_C/\mu_C \rangle = 1.9 \pm 1.0$. This value is close to the predictions of theoretical and numerical studies for a two-dimensional triangular network of identical springs.

histogram also shows two maxima at $\mu_C \sim 1.5$–3 μN/m and $\mu_C \sim 4.5$–5.5 μN/m (Fig. 7 *B*). From the fits we deduce the average values of elastic moduli for a single sheet $\langle K_C \rangle = 4.8 \pm 2.7$ μN/m and $\langle \mu_C \rangle = 2.4 \pm 0.7$ μN/m (Table 2). As expected, the skeleton shear modulus and the area expansion modulus have the same order of magnitude as the intact membrane shear modulus μ.

Fig. 8 represents a stack histogram of the ratio K_C/μ_C, K_C and μ_C being measured from the same deformation. From the 19 studied skeletons, 65 deformations give both μ_C and K_C. As expected, there is only one maximum. Fitting the stack histogram with a single Gaussian curve gives the average value $\langle K_C/\mu_C \rangle = 1.9 \pm 1.0$. This value is in agreement with the predictions of theoretical and numerical studies performed on networks either confined in two dimensions (Kantor and Nelson, 1987: $K_C/\mu_C = 2$; Boal et al., 1993: $K_C/\mu_C = 2$; Hansen et al., 1997: $K_C/\mu_C \leq 2$) or fluctuating in three dimensions (Boal, 1994: $K_C/\mu_C = 1.7$).

Measurements in isotonic buffer

We present here measurements held in an isotonic buffer without ATP at room temperature, i.e., ~25°C. The skeleton manipulation starts 5 min after its extraction. We apply the same kind of deformations as in the low hypotonic experiments.

Just after the lipid bilayer dissolution, the beads spontaneously move away from the trap centers, due to a partial shrinking of the skeleton (see Discussion). After rinsing out by a buffer injection the tension of the skeleton is partially released by decreasing the distance between the traps, and deformations can be held. During the manipulations, the optical tweezers keep the skeleton under slight tension to prevent further shrinkage as much as possible.

For each deformation we plot the expansion stress σ_e versus the relative surface increase $\Delta S/S$ and the shear stress σ_s versus the shear strain $u_{XX} - u_{YY}$. We obtain the same kind of graphs as the ones shown in Fig. 6, *A* and *B*. The surface increases by up to 15% and linear variations are observed in both cases. The slopes give the elastic moduli.

The experiments in isotonic buffer were held on 7 skeletons, 44 different deformations for K_C and 35 for μ_C. The average values over all the skeletons are $\langle K_C \rangle = 22.6 \pm 4.5$ μN/m, $\langle \mu_C \rangle = 7.9 \pm 2.7$ μN/m, and $\langle K_C/\mu_C \rangle = 2.9 \pm 0.6$. We have plotted in Fig. 9, *A* and *B* the stack histograms of K_C and μ_C obtained for each deformation. Contrary to the measurements in low osmolarity buffer, there is no clear evidence for two maxima on the stack histograms. It is

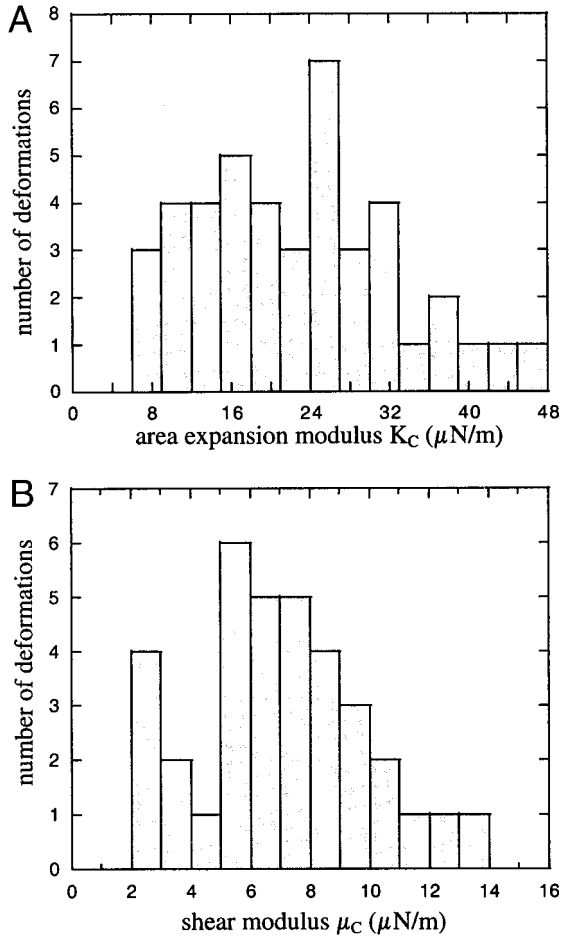

FIGURE 9 Stack histograms of the elastic moduli K_C (*A*) and μ_C (*B*) obtained for each deformation (44 measurements for K_C and 35 for μ_C on seven different skeletons) right after extraction in isotonic buffer. Contrary to the measurements in low osmolarity buffer, there is no clear evidence for two maxima. In this case the two sheets of the skeleton may be stuck together, because the high ionic strength of the medium screens the repulsive interaction between the spectrin filaments.

likely that the two sheets of the skeleton stick together because the high ionic strength of the medium screens the repulsive interaction between spectrin filaments. Fitting the K_C and μ_C stack histograms by a single Gaussian function

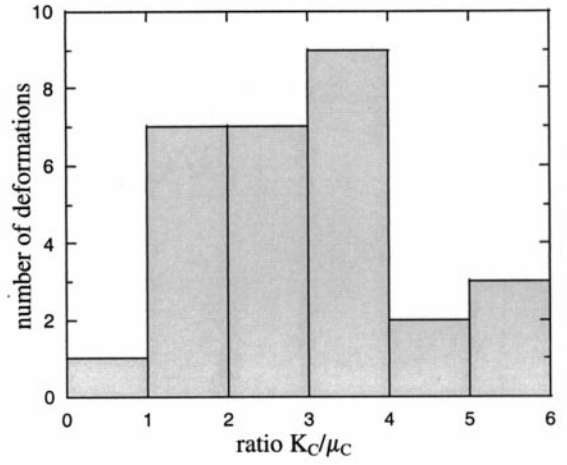

FIGURE 10 Stack histogram of the ratio K_C/μ_C, K_C, and μ_C being measured from the same deformation of a skeleton, right after extraction in isotonic buffer. The average value is $\langle K_C/\mu_C \rangle = 3.0 \pm 1.3$.

gives $\langle K_C \rangle = 21.3 \pm 10.5$ μN/m and $\langle \mu_C \rangle = 6.7 \pm 3.0$ μN/m. If we could assume that the two sheets were perfectly stuck to each other, with a density of adherence points comparable to the density of vertex in the spectrin network, then we could infer the elastic moduli for a single sheet: $\langle K_C \rangle = 10.7 \pm 5.3$ μN/m and $\langle \mu_C \rangle = 3.4 \pm 1.5$ μN/m. However, in practice, it is not possible to estimate the number of adherence points and we do not know how the stresses divide between the two sheets. Moreover, there might be a partial fusion between the two sheets, so that the spectrin network loses its initial topology. Nevertheless, we consider the above elastic moduli as orders of magnitude for a single sheet and we keep them for further comparison with the one measured in hypotonic buffer.

Fig. 10 shows the histogram of the ratio K_C/μ_C in isotonic buffer. As for the low hypotonic measurements, each value is determined on the same skeleton and for the same deformation. Of the 44 deformations held on the 7 skeletons, 24 give both K_C and μ_C. The average is $\langle K_C/\mu_C \rangle = 3.0 \pm 1.3$. This value is higher than the one expected from theoretical and numerical works (Kantor and Nelson, 1987; Boal et al., 1993; Boal, 1994; Hansen et al., 1996). This might result

TABLE 2 Comparison of the values of the area expansion and shear elastic modulus ascribed to a single sheet of the skeleton, measured in various conditions: low osmolarity buffer or isotonic buffer, right after extraction or 15 min after the first set of deformations

	Area Expansion Modulus K_C (μN/m)	Shear Modulus μ_C (μN/m)	K_C/μ_C
25 mOsm/kg buffer, no ATP, 25 mOsm/kg			
Right after extraction	4.8 ± 2.7 (88)	2.4 ± 0.7 (76)	1.9 ± 1.0 (65)
15 min after extraction	5.1 ± 1.2 (56)	2.0 ± 0.5 (38)	1.7 ± 1.0 (33)
Isotonic buffer, no ATP, 300 mOsm/kg			
Right after extraction	10.7 ± 5.3 (44)	3.4 ± 1.5 (35)	3.0 ± 1.3 (24)
15 min after extraction	15.4 ± 3.4 (35)	4.7 ± 1.3 (20)	3.7 ± 1.8 (18)

The total number of deformations is indicated in parentheses.

from the fact that the two sheets are stuck to each other and no longer form a plane triangular network.

Time dependence

After the first set of deformations, the skeleton is held for 10 or 15 min with the optical tweezers switched on. Then, another set of deformations is performed. The results, either in hypotonic or in isotonic buffer, are similar to the ones obtained right after the extraction: a linear dependence is observed between the stresses and strains, both for area expansion and shear. In the low osmolarity buffer, the stack histograms also present two maxima (not shown). We fit them by a sum of two Gaussian functions, and we deduce the elastic moduli for a single sheet in low osmolarity buffer $\langle K_C \rangle = 5.1 \pm 1.2$ μN/m and $\langle \mu_C \rangle = 2.0 \pm 0.5$ μN/m on, respectively, 56 and 38 deformations. The ratio $\langle K_C/\mu_C \rangle$ on 33 deformations is 1.7 ± 1.0. Thus, 15 min after the skeleton extraction in hypotonic buffer, we do not observe any significant change of its elastic coefficients. The values obtained in isotonic buffer are $\langle K_C \rangle = 15.4 \pm 3.4$ μN/m, $\langle \mu_C \rangle = 4.7 \pm 1.3$ μN/m, and $\langle K_C/\mu_C \rangle = 3.7 \pm 1.8$ on, respectively, 35, 20, and 18 deformations. We notice that, oppositely to hypotonic buffer, the skeleton properties rapidly change in isotonic buffer: after 15 min, the area expansion increases by up to 44% and the shear modulus by up to 38%. The spectrin filaments may progressively stick to each other as the buffer ions screen the repulsive interactions, and may finally form a three-dimensional structure, stiffer than a two-dimensional network.

The behavior at longer time is somehow different. Most of the time, we were able to manipulate a skeleton for 30 or 45 min after its extraction. The skeletons extracted in 25 mOsm/kg buffer generally become progressively softer with increasing time. Some measurements (data not shown) realized 30 min after extraction give an area expansion modulus as low as 1.5 μN/m—the shear modulus could not been measured. After 45 min, the skeletons are often damaged and can no longer be deformed. In some cases, they break up and separate from the beads. The long-time behavior of skeletons extracted in isotonic buffer is different. Generally, as long as the skeleton is held under tension with the tweezers, the stiffness stabilizes after 15 min and no further apparent change is measured.

ATP dependence

Previous work have shown that the mechanical behavior of the RBC membrane is modified in the presence of adenosine triphosphate (ATP) (Manno et al., 1995). For instance, ATP enhances the fluctuations of the intact membrane (Levin and Korenstein, 1991) and also of the membrane skeleton (Tuvia et al. 1998), with which it interacts through various binding sites. In this work we looked for a possible change of the skeleton elasticity in the presence of ATP. Measurements are performed in low osmolarity buffer (25 mOsm/kg) with 1 mM ATP. We notice that, after extraction, the skeletons are generally under tension, while no tension is observed on skeletons extracted in low osmolarity buffer without ATP. We must release this tension by reducing the distance between the traps before pulling on the skeletons. The area expansion modulus measured right after extraction and averaged over eight different deformations of four skeletons is $\langle K_C \rangle = 11.0 \pm 4.5$ μN/m. Although there are too few results to infer a reliable value for the elastic moduli of a single sheet, it seems that adding ATP increases the initial tension without significantly changing the elastic moduli.

DISCUSSION

Despite the relative dispersion of the values from one skeleton to another and the variations observed when changing the experimental conditions, all the above results show a relative consistency: both the area expansion and shear moduli have the expected order of magnitude and their ratio is quite comparable to the theoretical predictions. This strengthens the reliability of the technique used to deform the skeletons and the validity of the theoretical approach built to analyze the data.

Nevertheless, the dispersion of the measurements from one skeleton to another and even, for a same skeleton, from one kind of deformation to the other (Table 1) has to be explained. It may have several origins:

1. The RBC has a finite lifetime of ~120 days. Many modifications take place in its membrane during this time, among them an increase in the membrane elastic coefficients (Linderkamp and Meiselman, 1982). A recent work (Corsi et al., 1999) has highlighted modifications of α-spectrin during the cell lifetime. The dispersion of the measurements from one skeleton to another can partially be explained by different ages of the skeletons. Variations in the skeleton structure, including variations of the defect density, are a further source of natural dispersion;
2. It has been pointed out that, depending on the bead position at the periphery of the membrane, the deformation may concern either a single sheet or both sheets of the skeleton (Fig. 4). But it may also happen that the two sheets of the skeleton stick together (double counting), or that one of them tears up (single counting), independently of the bead positions. It is even likely that, for the same skeleton, the deformation may be exerted against either one or two sheets, depending on the nature and orientation of the applied forces (pure expansion, pure shear, or a combination of both). This led us to show on a same histogram the values of K_C and μ_C obtained for each deformation (Figs. 7 and 9). For the experiments

performed in low osmolarity buffer, the histograms present two maxima, which supports the above interpretation;

3. Variations in the extent of the binding region between the bead and the skeleton is also a possible cause for the dispersion. In this region, the strains and stresses are probably not homogeneous. This effect, which cannot be handled in our analytical theory, may affect the measured values of the elastic coefficients.

One question arising from this study is the difference between a free network and a network embedded into a lipid membrane. We have noticed that, at least in isotonic buffer, the skeleton shrinks after extraction. This is likely due to the larger number of degrees of freedom associated with fluctuations in the third dimension, and thus supports the idea that the skeleton behaves like a three-dimensional fluctuating object. On the contrary, the extracted skeleton slightly expands in hypotonic buffer. In this case, two effects may compensate the shrinking related to fluctuations: the increase of the spectrin persistence length and the possible existence of a pre-stressed state imposed by the lipid bilayer (Svoboda et al., 1992; Discher et al., 1998).

It is interesting to compare the measured values of K_C and μ_C to various predictions found in the literature. Monte Carlo simulations performed on such a free network led to estimates for the network elastic coefficients, namely $\mu_C = 10 \pm 2$ μN/m and $K_C = 17 \pm 2$ μN/m (Boal, 1994). These values are larger than our experimental ones in isotonic buffer, but at this stage the agreement is reasonable. Other models relate the macroscopic elastic constants to the stiffness k of a single spectrin filament (Kantor and Nelson, 1987; Boal et al., 1993):

$$K_C = 2\mu_C = \frac{\sqrt{3}}{2} k \tag{6}$$

Although this formula applies to a purely two-dimensional triangular network without defect, an estimate of k can be inferred from our data. In our experiments, the forces exerted on the skeleton (1-8 pN) are definitely too small to allow unfolding of spectrin subunits, for which the required forces per strand are of the order of 25-35 pN (Rief et al., 1999), or 60 pN (Lenne et al., 2000), depending on the nature of the repeats and on the pulling speed. Thus, we assume that the elastic behavior of spectrin tetramers is purely entropic. Therefore, it is possible to relate k to the persistence length ξ of a single spectrin oligomer, and to its maximum extension L, through the worm-like chain model (Marko and Siggia, 1995). In the low stretching limit, one has:

$$k = \frac{3k_B T}{2\xi L} \tag{7}$$

Taking $L \sim 200$ nm and $\langle K_C \rangle \sim 5$ μN/m, as found in hypotonic buffer, we can estimate the persistence length of a spectrin filament: $\xi \sim 5$ nm. This is a quite reasonable value, comparable to the estimate given by Svoboda et al. (1992) from measurements on a free skeleton: $\xi \sim 6$ nm. Although the worm-like chain model applies to a free polymer not included in a network, it should give the right order of magnitude for k. Recent simulations (Discher et al., 1998), extending the single chain model to networks, support this assumption.

As mentioned in the Results section, the skeleton partially collapses in isotonic buffer and its structure is probably modified, which makes it difficult to compare the results between isotonic and low osmolarity buffers. Based on values given in Table 2, the area expansion and shear moduli ascribed to a single sheet become greater when the ionic strength of the medium is increased. Svoboda et al. (1992) have also reported that the skeleton gets stiffer as the ionic strength increases. According to Eq. 7, this is consistent with a decrease of the persistence length ξ. It is also likely that the screening of the spectrin-spectrin repulsive interaction causes new in-plane links between the filaments, which lowers the average end-to-end distance L and increases the stiffness.

Concerning the time evolution after extraction, the observation in low osmolarity buffer is a slow decrease of the elastic moduli, noticeable about 30 min after extraction. This does not necessarily mean that the network becomes intrinsically softer. It is likely that one observes a denaturation of the skeleton, either localized at the complex junctions between the spectrin tetramers, or in the tetramers themselves, or even at the binding sites of the skeleton to the silica beads. On the contrary, in isotonic buffer, the stiffness rapidly increases, probably as the spectrin filaments progressively stick together.

At this preliminary stage it is difficult to give a properly supported interpretation of the measurements obtained with ATP. It seems that ATP increases the tension of the skeleton without significant change of its elastic coefficients. A possible explanation is that, as for the intact membrane, ATP enhances the out-of-plane skeleton fluctuations without modifying its in-plane elastic properties. Further measurements will be necessary to confirm or invalidate this hypothesis.

CONCLUSION

For the first time, both the area expansion and the shear moduli of freshly extracted RBC skeletons have been measured in controlled experimental conditions: in low hypotonic buffer or isotonic buffer, right after extraction or after waiting for a possible time evolution, with and without ATP. All the measurements are consistent and in good agreement with models describing the mechanical behavior of such a polymer network. The most prominent results concern the elastic moduli of the skeleton in low osmolarity buffer, which is an appropriate condition to study the be-

havior of the isolated two-dimensional network. The area expansion and shear moduli are, respectively, $\langle K_C \rangle = 4.8 \pm 2.7$ μN/m and $\langle \mu_C \rangle = 2.4 \pm 0.7$ μN/m. In such conditions, the ratio $\langle K_C/\mu_C \rangle$ is found equal to 1.9 ± 1.0, in good agreement with theoretical and numerical predictions for a triangular network of identical springs. After 30–45 min, denaturation of the structure leads to a mechanical softening. In isotonic buffer, the area expansion modulus is greater, because the two sheets of the skeleton stick together and because the stiffness of each spectrin filament is larger. A major improvement of the technique would be to take into account the actual deformation of the skeleton to extract the elastic moduli and check to which extent the assumptions introduced for the data analysis are fulfilled. However, this is not expected to significantly change the values of the area expansion and shear moduli.

APPENDIX

This part details the algebra and the constructions used to relate the forces ($\mathbf{F}_A$, $\mathbf{F}_B$, $\mathbf{F}_C$) exerted at the vertices A, B, C of a triangular membrane to the components of the 2×2 stress tensor $[\boldsymbol{\sigma}]$ introduced in the main text. The membrane is assumed to be a purely two-dimensional, plane, continuous, homogeneous and isotropic elastic medium. The model is restricted to small deformations, so the equations of linear elasticity apply. Moreover, the stress and strain tensors are assumed to be homogeneous over the membrane.

The mechanical equilibrium of the membrane is written as:

$$\mathbf{F}_A + \mathbf{F}_B + \mathbf{F}_C = \mathbf{0} \tag{A1}$$

and

$$\mathbf{M}(\mathbf{F}_A) + \mathbf{M}(\mathbf{F}_B) + \mathbf{M}(\mathbf{F}_C) = \mathbf{0} \tag{A2}$$

where $\mathbf{M}$ is the force momentum calculated at a given point of the plane. Equation A2 is equivalent to the condition that the three straight lines supporting the forces intersect at a single point (Fig. 3). In the following, we determine the configuration of the forces $\mathbf{F}_A$, $\mathbf{F}_B$, and $\mathbf{F}_C$ and the associated stresses, in the cases of a pure area expansion deformation, of a pure shear deformation and finally in the most general case (shear + expansion).

Pure area expansion stress

For a limited surface, the relation between the force d$\mathbf{G}$ exerted on an element dl of its boundary and the stress tensor $[\boldsymbol{\sigma}]$ is:

$$\mathrm{d}\mathbf{G} = [\boldsymbol{\sigma}]\mathbf{n}\mathrm{d}l \tag{A3}$$

Here the unit vector $\mathbf{n}$ defines the external normal to the element of length dl. In the case of pure area expansion, $[\boldsymbol{\sigma}]$ is diagonal and may be written as $[\boldsymbol{\sigma}] = \sigma_e\,[\mathbf{I}]$, where $[\mathbf{I}]$ is the identity matrix. The resultant force exerted on a segment of length L is $\mathbf{G} = \sigma_e L\,\mathbf{n}$. In the case of a triangle ABC, the forces $\mathbf{G}_A$, $\mathbf{G}_B$, and $\mathbf{G}_C$ generating a pure expansion are respectively oriented along the normals to the segments BC, CA, and AB (Fig. 11 *A*). Their sum $\mathbf{G}_A + \mathbf{G}_B + \mathbf{G}_C$ is zero and their amplitudes are related to the stress σ_e by:

$$\sigma_e = \frac{G_A}{BC} = \frac{G_B}{AC} = \frac{G_C}{AB} \tag{A4}$$

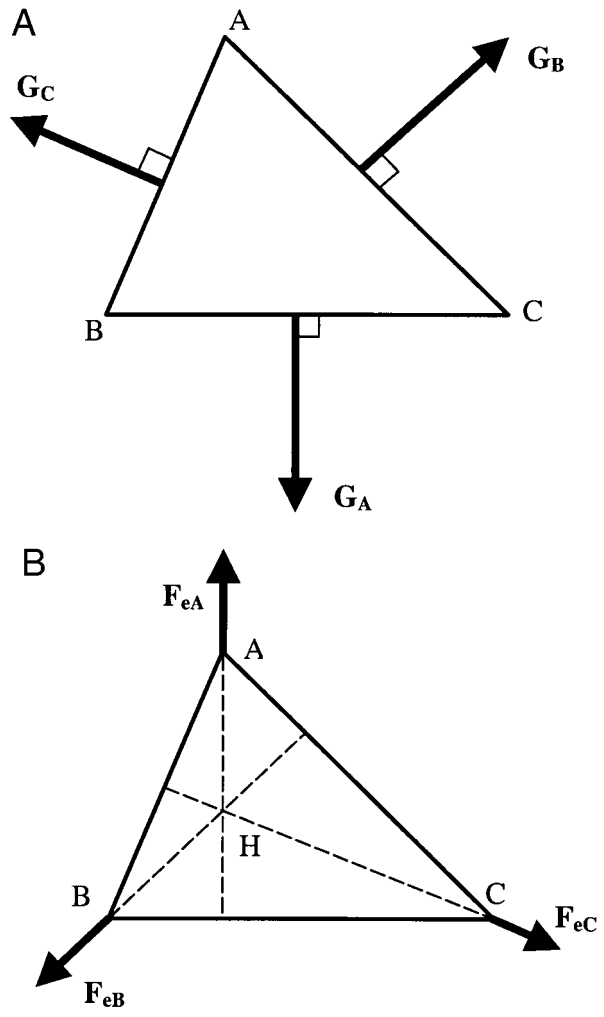

FIGURE 11 (*A*) Configuration of three forces $\mathbf{G}_A$, $\mathbf{G}_B$, and $\mathbf{G}_C$ generating a pure expansion stress on the triangle ABC. They are oriented along the normals to the segments BC, CA, and AB, and their sum $\mathbf{G}_A + \mathbf{G}_B + \mathbf{G}_C$ is zero. (*B*) The three forces $\mathbf{F}_{eA}$, $\mathbf{F}_{eB}$, and $\mathbf{F}_{eC}$ applied at the vertices A, B, and C exert a pure expansion stress equivalent to the one generated by $\mathbf{G}_A$, $\mathbf{G}_B$, and $\mathbf{G}_C$. They are supported by the triangle heights and their amplitude is given by equations A5–A7.

For an elementary triangle ABC of surface dS, it is equivalent to replace the force $\mathbf{G}_A$ exerted in the middle of BC by a pair of two forces equal to $\mathbf{G}_A/2$, exerted in B and in C. This construction also holds for a triangle ABC of finite surface, as soon as the strain and the stress are assumed homogeneous over the triangle. Similar constructions are valid in B and C for $\mathbf{G}_B$ and $\mathbf{G}_C$. Then $\mathbf{G}_A$, $\mathbf{G}_B$, and $\mathbf{G}_C$ can be replaced by three forces $\mathbf{F}_{eA}$, $\mathbf{F}_{eB}$, and $\mathbf{F}_{eC}$ exerted at the vertices A, B, and C, generating the same stress σ_e and given by (see Fig. 11 *B*):

$$\mathbf{F}_{eA} = \frac{\mathbf{G}_B + \mathbf{G}_C}{2} = -\frac{\mathbf{G}_A}{2} \tag{A5}$$

$$\mathbf{F}_{eB} = \frac{\mathbf{G}_C + \mathbf{G}_A}{2} = -\frac{\mathbf{G}_B}{2} \tag{A6}$$

$$\mathbf{F}_{eC} = \frac{\mathbf{G}_A + \mathbf{G}_B}{2} = -\frac{\mathbf{G}_C}{2} \tag{A7}$$

Their amplitudes are related to σ_e by:

$$\sigma_e = 2\frac{F_{eA}}{BC} = 2\frac{F_{eB}}{AC} = 2\frac{F_{eC}}{AB} \quad \text{(A8)}$$

In conclusion, the forces $\mathbf{F}_{eA}$, $\mathbf{F}_{eB}$, and $\mathbf{F}_{eC}$ generating a pure area expansion are supported by the triangle heights, intersecting at point H, and their sum is zero.

Pure shear stress

For a pure shear stress there is a system of coordinates ($\mathbf{e}_X$, $\mathbf{e}_Y$) (called the principal system of coordinates in the following) in which $[\boldsymbol{\sigma}]$ is diagonal and may be written as $[\boldsymbol{\sigma}] = \sigma_s[\mathbf{J}]$, with $[\mathbf{J}] = \begin{bmatrix} 1 & 0 \\ 0 & -1 \end{bmatrix}$. The resultant forces $\mathbf{K}_A$, $\mathbf{K}_B$, and $\mathbf{K}_C$ exerted on the respective sides BC, CA, and AB are given by integrating Eq. A3 and are represented in Fig. 12 *A*. The direction of $\mathbf{K}_A$ is such that the angles ($\mathbf{n}_A$, $\mathbf{e}_X$) and ($\mathbf{e}_X$, $\mathbf{K}_A$) are equal (here $\mathbf{n}_A$ represents the unit vector normal to BC and directed out of the triangle). The same construction applies for $\mathbf{K}_B$ and $\mathbf{K}_C$. As in the pure area expansion case, their respective amplitudes are related to the shear stress σ_s by:

$$\sigma_s = \frac{K_A}{BC} = \frac{K_B}{AC} = \frac{K_C}{AB} \quad \text{(A9)}$$

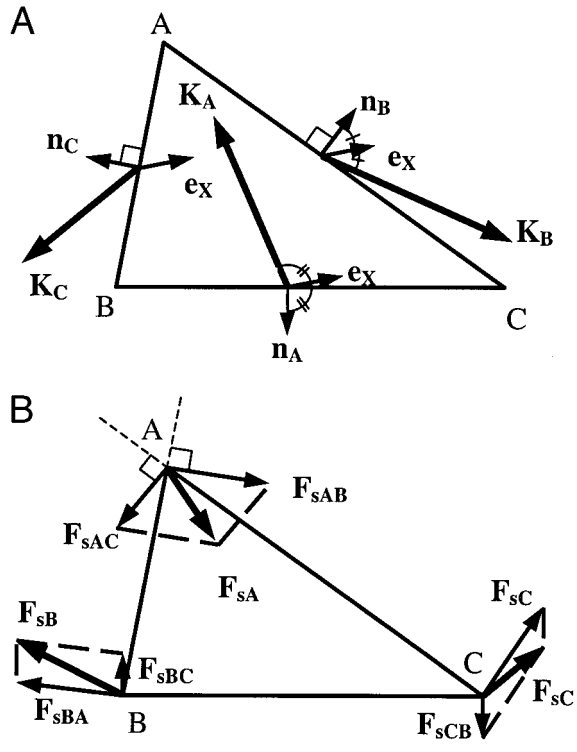

FIGURE 12 (*A*) Configuration of three forces $\mathbf{K}_A$, $\mathbf{K}_B$, and $\mathbf{K}_C$ generating a pure shear stress on the triangle ABC. Their sum $\mathbf{K}_A + \mathbf{K}_B + \mathbf{K}_C$ is zero. They are oriented in such a way that the angles ($\mathbf{n}_A$, $\mathbf{e}_X$) and ($\mathbf{e}_X$, $\mathbf{K}_A$) are equal (and equivalent relations by permutation). (*B*) The three forces $\mathbf{F}_{sA}$, $\mathbf{F}_{sB}$, and $\mathbf{F}_{sC}$ applied at the vertices A, B, and C exert a pure shear stress equivalent to the one generated by $\mathbf{K}_A$, $\mathbf{K}_B$, and $\mathbf{K}_C$. They intersect at a single point located on the circle passing through the points A, B, and C, and their amplitude is given by equations A10–A12. They are the result of the superposition of three torques ($\mathbf{F}_{sAB}$, $\mathbf{F}_{sBA} = -\mathbf{F}_{sAB}$), ($\mathbf{F}_{sAC}$, $\mathbf{F}_{sCA} = -\mathbf{F}_{sAC}$), and ($\mathbf{F}_{sBC}$, $\mathbf{F}_{sCB} = -\mathbf{F}_{sBC}$).

Following the same procedure as above, an equivalent configuration is obtained by replacing $\mathbf{K}_A$ by a pair of two forces equal to $\mathbf{K}_A/2$, exerted in B and C, and similar constructions for $\mathbf{K}_B$ and $\mathbf{K}_C$. The equivalent forces exerted in A, B, and C are, respectively:

$$\mathbf{F}_{sA} = \frac{\mathbf{K}_B + \mathbf{K}_C}{2} = -\frac{\mathbf{K}_A}{2};\ \sigma_s = 2\frac{F_{sA}}{BC} \quad \text{(A10)}$$

$$\mathbf{F}_{sB} = \frac{\mathbf{K}_C + \mathbf{K}_A}{2} = -\frac{\mathbf{K}_B}{2};\ \sigma_s = 2\frac{F_{sB}}{AC} \quad \text{(A11)}$$

$$\mathbf{F}_{sC} = \frac{\mathbf{K}_A + \mathbf{K}_B}{2} = -\frac{\mathbf{K}_C}{2};\ \sigma_s = 2\frac{F_{sC}}{AB} \quad \text{(A12)}$$

Due to the orientation of $\mathbf{F}_{sA}$, $\mathbf{F}_{sB}$, and $\mathbf{F}_{sC}$, the angles ($\mathbf{F}_{sA}$, $\mathbf{F}_{sB}$) and (**CA**, **CB**) are equal. Similar relations are obtained by permutation. As a consequence, the three forces intersect at a single point located on the circle drawn around the triangle ABC.

Another useful transformation consists in splitting this triplet of forces into a set of three torques. In A for instance, one projects $\mathbf{F}_{sA}$ onto the normals $\mathbf{n}_B$ and $\mathbf{n}_C$ to the sides AC and AB. The same construction in B and C leads to (see Fig. 12 *B*):

$$\mathbf{F}_{sA} = \mathbf{F}_{sAC} + \mathbf{F}_{sAB} \quad \text{(A13)}$$

$$\mathbf{F}_{sB} = \mathbf{F}_{sBA} + \mathbf{F}_{sBC} \quad \text{(A14)}$$

$$\mathbf{F}_{sC} = \mathbf{F}_{sCB} + \mathbf{F}_{sCA} \quad \text{(A15)}$$

Using the mechanical equilibrium condition $\mathbf{F}_{sA} + \mathbf{F}_{sB} + \mathbf{F}_{sC} = \mathbf{0}$, the equality between the angles ($\mathbf{n}_A$, $\mathbf{e}_X$) and ($\mathbf{e}_X$, $\mathbf{F}_{sA}$), and the relations obtained by permutation, it is possible to show that $\mathbf{F}_{sAC} = -\mathbf{F}_{sCA}$, $\mathbf{F}_{sAB} = -\mathbf{F}_{sBA}$, and $\mathbf{F}_{sBC} = -\mathbf{F}_{sCB}$ (the geometrical demonstration presents no difficulty). Consequently, the configuration of forces generating a pure shear stress may be seen as a triplet of torques ($\mathbf{F}_{sAB}$, $-\mathbf{F}_{sAB}$), ($\mathbf{F}_{sAC}$, $-\mathbf{F}_{sAC}$) and ($\mathbf{F}_{sBC}$, $-\mathbf{F}_{sBC}$), respectively, exerted on the sides AB, AC, and BC, as shown in Fig. 12 *B*.

General case: simultaneous expansion and shear stress

In the most general case, one can use the tools developed in the above sections to calculate the stresses associated to the three forces ($\mathbf{F}_A$, $\mathbf{F}_B$, $\mathbf{F}_C$). As shown in the main text and in Fig. 3, the first step is to project $\mathbf{F}_A = \mathbf{F}_{AB} + \mathbf{F}_{AC}$ along the normals $\mathbf{n}_C$ and $\mathbf{n}_B$ to AB and AC, and make the equivalent constructions in B and C. The pair of forces ($\mathbf{F}_{AB}$, $\mathbf{F}_{BA}$) is then split into a pair of identical forces ($-\mathbf{F}_{eC}$, $-\mathbf{F}_{eC}$) exerted in A and in B, and a torque ($\mathbf{F}_{sAB}$, $\mathbf{F}_{sBA} = -\mathbf{F}_{sAB}$), defined by:

$$\mathbf{F}_{AB} = -\mathbf{F}_{eC} + \mathbf{F}_{sAB} \quad \mathbf{F}_{BA} = -\mathbf{F}_{eC} + \mathbf{F}_{sBA} = -\mathbf{F}_{eC} - \mathbf{F}_{sAB} \quad \text{(A16)}$$

Similar definitions are obtained by permutation:

$$\mathbf{F}_{AC} = -\mathbf{F}_{eB} + \mathbf{F}_{sAC} \quad \mathbf{F}_{CA} = -\mathbf{F}_{eB} + \mathbf{F}_{sCA} = -\mathbf{F}_{eB} - \mathbf{F}_{sAC} \quad \text{(A17)}$$

$$\mathbf{F}_{BC} = -\mathbf{F}_{eA} + \mathbf{F}_{sBC} \quad \mathbf{F}_{CB} = -\mathbf{F}_{eA} + \mathbf{F}_{sCB} = -\mathbf{F}_{eA} - \mathbf{F}_{sBC} \quad \text{(A18)}$$

The three forces $\mathbf{F}_{eA}$, $\mathbf{F}_{eB}$, and $\mathbf{F}_{eC}$ are oriented toward the normals $\mathbf{n}_A$, $\mathbf{n}_B$, and $\mathbf{n}_C$. Moreover, like $\mathbf{F}_A$, $\mathbf{F}_B$, and $\mathbf{F}_C$, their sum is zero. Then, according to the first section, they generate a pure area expansion stress of amplitude σ_e given by Eq. A8.

In the same way, the three torques ($\mathbf{F}_{sAB}$, $\mathbf{F}_{sBA}$), ($\mathbf{F}_{sAC}$, $\mathbf{F}_{sCA}$) and ($\mathbf{F}_{sBC}$, $\mathbf{F}_{sCB}$) generate a pure shear stress. The equivalent forces exerted in A, B, and C are $\mathbf{F}_{sA}$, $\mathbf{F}_{sB}$, and $\mathbf{F}_{sC}$ given by Eqs. A13–A15 and the amplitude σ_s is determined from formulas A10–A12:

$$\sigma_s = 2\frac{\|\mathbf{F}_{sA}\|}{BC} = \frac{\|\mathbf{F}_A - \mathbf{F}_{BA} - \mathbf{F}_{CA}\|}{BC} \qquad \text{(A19)}$$

and equivalent relations by permuting A, B, and C. As in the second section, the axes of the principal system of coordinates ($\mathbf{e}_X$, $\mathbf{e}_Y$) are determined by writing the equality of the two angles ($\mathbf{n}_A$, $\mathbf{e}_X$) and ($\mathbf{e}_X$, $-\mathbf{F}_{sA}$).

REFERENCES

Aronovitz, J. A., and T. C. Lubensky. 1988. Fluctuations of solid membranes. *Phys. Rev. Lett.* 60:2634–2637.

Bennett, V., and D. M. Gilligan. 1993. The spectrin-based membrane skeleton and micron-scale organization of the plasma membrane. *Annu. Rev. Cell Biol.* 9:27–66.

Boal, D. H. 1994. Computer simulation of a model network for the erythrocyte cytoskeleton. *Biophys. J.* 67:521–529.

Boal, D. H., U. Seifert, and J. C. Shillcock. 1993. Negative Poisson ratio in two-dimensional networks under tension. *Phys. Rev. E.* 48: 4274–4283.

Corsi, D., M. Paiardini, R. Crinelli, A. Bucchini, and M. Magnani. 1999. Alteration of α-spectrin ubiquitination due to age dependent changes in the erythrocyte membrane. *Eur. J. Biochem.* 261:775–783.

Discher, D. E., D. H. Boal, and S. K. Boey. 1998. Simulations of the erythrocyte cytoskeleton at large deformation. II. Micropipette aspiration. *Biophys. J.* 75:1584–1597.

Discher, D. E., N. Mohandas, and E. A. Evans. 1994. Molecular maps of red blood cell deformation: hidden elasticity and in situ connectivity. *Science.* 266:1032–1035.

Engelhardt, H., and E. Sackmann. 1988. On the measurement of shear elastic moduli and viscosities of erythrocyte plasma membranes by transient deformation in high frequency electric fields. *Biophys. J.* 54: 495–508.

Evans, E. A. 1973. New membrane concept applied to the analysis of fluid shear- and micropipette-deformed red blood cells. *Biophys. J.* 13: 941–954.

Evans, E. A. 1983. Bending elastic modulus of red blood cell membrane derived from buckling instability in micropipette aspiration tests. *Biophys. J.* 43:27–30.

Hansen, J. C., R. Skalak, S. Chien, and A. Roger. 1996. An elastic network based on the structure of the red blood cell membrane skeleton. *Biophys. J.* 13:146–166.

Hansen, J. C., R. Skalak, S. Chien, and A. Roger. 1997. Influence of the network topology on the elasticity of the red blood cell membrane skeleton. *Biophys. J.* 72:2369–2381.

Hénon, S., G. Lenormand, A. Richert, and F. Gallet. 1999. A new determination of the shear modulus of the human erythrocyte membrane using optical tweezers. *Biophys. J.* 76:1145–1151.

Hochmuth, R. M., and R. E. Waugh. 1987. Erythrocyte membrane elasticity and viscosity. *Annu. Rev. Physiol.* 49:209–219.

Kantor, Y., and D. R. Nelson. 1987. Phase transition in flexible polymeric surfaces. *Phys. Rev. A.* 36:4020–4032.

Lelièvre, J. C., C. Bucherer, S. Geiger, C. Lacombe, and V. Vereycken. 1995. Blood cell biomechanics evaluated by the single-cell micromanipulation. *J. Phys. III France.* 5:1689–1706.

Lenne, P.-F., A. J. Raae, S. M. Altmann, M. Saraste, and J. K. H. Hörber. 2000. States and transitions during unfolding of a single spectrin repeat. *FEBS Lett.* 476:124–128.

Levin, S. V., and R. Korenstein. 1991. Membrane fluctuations in erythrocytes are linked to MgATP-dependent dynamic assembly of the membrane skeleton. *Biophys. J.* 60:733–737.

Linderkamp, O., and H. J. Meiselman. 1982. Geometric, osmotic, and membrane mechanical properties of density-separated human red blood cells. *Blood.* 59:1121–1127.

Liu, Y., D. K. Cheng, G. J. Sonek, M. W. Berns, C. F. Chapman, and B. J. Tromberg. 1995. Evidence for localized cell heating induced by infrared optical tweezers. *Biophys. J.* 68:2137–2144.

Liu, S., L. Derick, and J. Paleck. 1987. Visualization of the hexagonal lattice in the erythrocyte membrane skeleton. *J. Cell Biol.* 104:527–536.

Manno, S., Y. Takakuwa, K. Nagao, and N. Mohandas. 1995. Modulation of erythrocyte membrane mechanical functions by β-spectrin phosphorylation and dephosphorylation. *J. Biol. Chem.* 270:5659–5665.

Marko, J., and E. Siggia. 1995. Stretching DNA. *Macromolecules.* 28: 8759–8770.

Mohandas, N., and E. Evans. 1994. Mechanical properties of the red cell membrane in relation to molecular structure and genetic defects. *Annu. Rev. Biophys. Biomol. Struct.* 23:787–818.

Peterson, M. A., H. Strey, and E. Sackmann. 1992. Theoretical and phase contrast microscopic eigenmode analysis of erythrocyte flicker: amplitudes. *J. Phys. II France.* 2:1273–1285.

Rief, M., J. Pascual, M. Saraste, and H. E. Gaub. 1999. Single molecule force spectroscopy of spectrin repeats: low unfolding forces in helix bundles. *J. Mol. Biol.* 286:553–561.

Simmons, R. M., J. T. Finer, S. Chu, and J. A. Spudish. 1996. Quantitative measurements of force and displacement using an optical trap. *Biophys. J.* 70:1813–1822.

Stokke, B. T., A. Mikkelsen, and A. Elgsaeter. 1986. The human erythrocyte membrane may be an ionic gel. III. Micropipette aspiration of unswollen erythrocytes. *J. Theor. Biol.* 123:205–211.

Svoboda, K., and S. M. Block. 1994. Biological applications of optical forces. *Annu. Rev. Biophys. Biomol. Struct.* 23:247–285.

Svoboda, K., C. F. Schmidt, D. Branton, and S. M. Block. 1992. Conformation and elasticity of the isolated red blood cell membrane skeleton. *Biophys. J.* 63:784–793.

Tuvia, S., S. Levin, A. Bitler, and R. Korenstein. 1998. Mechanical fluctuations of the membrane-skeleton are dependent on F-actin ATPase in human erythrocytes. *J. Cell. Biol.* 141:1551–1561.

Ursitti, J. A., D. W. Pumplin, J. B. Wade, and R. J. Bloch. 1991. Ultrastructure of the human erythrocyte cytoskeleton and its attachment to the membrane. *Cell Motil. Cytoskeleton.* 19:227–243.

Ursitti, J. A., and J. B. Wade. 1993. Ultrastructure and immunocytochemistry of the isolated human erythrocyte membrane skeleton. *Cell Motil. Cytoskeleton.* 25:30–42.

Yu, J., D. A. Fishman, and T. L. Steck. 1973. Selective solubilization of proteins and phospholipids from red blood cell membranes by non-ionic detergents. *J. Supramol. Struct.* 1:233–248.